

# Emergent Berezinskii-Kosterlitz-Thouless and Kugel-Khomskii physics in the triangular lattice bilayer colbaltate

Gang V. Chen

*International Center for Quantum Materials, School of Physics, Peking University, Beijing 100871, China and Collaborative Innovation Center of Quantum Matter, 100871, Beijing, China*

Motivated by the experiments on the triangular lattice bilayer colbaltate  $\text{K}_2\text{Co}_2(\text{SeO}_3)_3$ , we consider an extended XXZ model to explore the underlying physics from a couple observation. The model is composed of interacting  $\text{Co}^{2+}$  dimers on the triangular lattice, where the  $\text{Co}^{2+}$  ion provides an effective spin-1/2 local moment via the spin-orbit coupling and the crystal field effect. The intra-dimer interaction is dominant and would simply favor the local spin singlet, and the inter-dimer interactions compete with the inter-dimer interaction, leading to rich behaviors. With the easy-axis anisotropy, it is shown that, in the ground state manifold of the intra-dimer Ising interaction, the system realizes an effective quantum Ising model, where the ground state is either a 3-sublattice order with a mixture of antiferromagnetic Ising order and a valence-bond spin singlet or Ising disordered. The finite temperature regime realizes the Berezinskii-Kosterlitz-Thouless physics. To explore the full excitations, we incorporate the excited state manifold of the intra-dimer Ising interaction and establish the emergent Kugel-Khomskii physics. Thus, the triangular lattice bilayer colbaltate is an excellent platform to explore the interplay between geometrical frustration and anisotropic interactions as well as the emergent effective models and the resulting physics.

Frustrated magnets have been an active field in modern condensed matter physics [1]. Frustration arises from competing interaction that cannot be optimized simultaneously. A common source of frustration is the geometrical frustration on frustrated lattices such as triangular, kagomé, and pyrochlore lattices. The study of frustrated magnets on these frustrated lattices has contributed to a large portion of topics. Theoretically, frustration generates a large number of degenerate and nearly degenerate many-body states on which the sub-dominant interactions are reduced to effective interaction and then lead to rather interesting and exotic behaviors. Thus, the ingredient of frustration has inspired many contrived theoretical models and works in last two decades. On the other hand, the abundance of frustrated magnetic materials has provided the experimental motivation for new frustrated models and phenomena out of the frustration.

One ongoing interest on the frustrated materials is about the spin-orbit-coupled Mott insulators [2]. These materials are often the  $4d/5d$  transition metal compounds and  $4f$  rare-earth magnets. In these systems, due to the spin-orbit coupling and the electron correlation, the magnetic interactions are often quite anisotropic, both in the spin space and the position space. The resulting models may often differ significantly from simple Heisenberg models, and these anisotropic models may carry strong frustration even on unfrustrated lattices. The representative example is the honeycomb lattice Kitaev model that has the relevance on various iridates and  $\alpha\text{-RuCl}_3$  [3]. With both anisotropy and frustration, it is natural to expect that these anisotropic and frustrated models on geometrically frustrated lattices could bring more unexpected behaviors. Much progress has been made in the rare-earth pyrochlore magnets [4] and the  $4d/5d$  Kitaev materials [3].

Some of the recent attention has been directed to the colbaltates. One motivation was to explore the Kitaev interaction and Kitaev spin liquid among the honeycomb colbaltates where the spin-orbit coupling plays a similar role as the one for the iridates and induces the anisotropic interactions, and the progress has been made in the honeycomb magnets  $\text{Na}_2\text{Co}_2\text{TeO}_6$  and  $\text{Na}_3\text{Co}_2\text{SbO}_6$  [5, 6]. In fact, the spin-orbit coupling can sometimes play an important role for the underlying physics even in the  $3d$  transition metal compounds, and this differs from elements to elements and depends on the crystal environments. Moreover, several colbaltates are long known to be good realizations of the anisotropic models such as the quantum Ising model as the extreme. These include the quasi-1D Ising magnets  $\text{CoNb}_2\text{O}_6$  [7–9],  $\text{BaCo}_2\text{V}_2\text{O}_8$  [10–12], and  $\text{SrCo}_2\text{V}_2\text{O}_8$  [13] where not only the external field gives a useful tunability of the quantum phases but also the system could produce emergent and exotic excitations associated with the criticality [7, 14].

We are inspired by the experiments on the Co-dimer

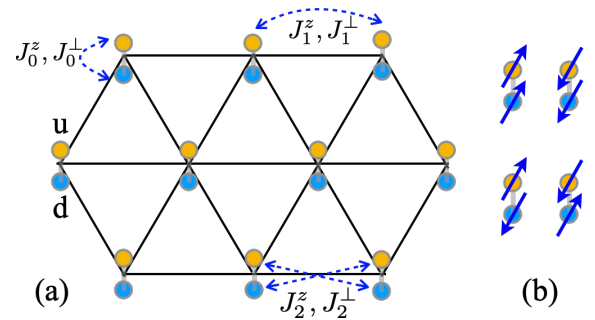


FIG. 1. (a) The  $\text{Co}^{2+}$  dimers form a triangular lattice. (b) Two anticollinear and two collinear spin configurations on the dimer, where the spins point along the  $\pm z$  direction.

$S_{ui}^z$	$S_{ui}^x$	$S_{ui}^y$	$S_{di}^z$	$S_{di}^x$	$S_{di}^y$	$S_{ui}^z S_{di}^z$	$S_{ui}^x S_{di}^x + S_{ui}^y S_{di}^y$
$\tau_i^z$	0	0	$-\tau_i^z$	0	0	$-\frac{1}{4}$	$\tau_i^x$
$\tau_i^z$	$2\tau_i^x \mu_i^x$	$2\tau_i^y \mu_i^x$	$2\tau_i^z \mu_i^z$	$\mu_i^x$	$2\tau_i^z \mu_i^y$	$\frac{\mu_i^z}{2}$	$\tau_i^x (\frac{1}{2} - \mu_i^z)$

TABLE I. The list of spin operators on each dimer under different representations. The first line is the original spin operator on the local lattice site. The second line is in terms of the pseudospin  $\tau_i^\mu$  after being projected onto the ground state manifold of the intra-dimer Ising interaction. The third line is in terms of the pseudospin  $\tau_i^\mu$  and  $\mu_i^\nu$  after including all the local states of the dimer. The prescription is described in the main text.

triangular lattice antiferromagnet  $\text{K}_2\text{Co}_2(\text{SeO}_3)_3$  [15]. As it is shown in Fig. 1, the two neighboring  $\text{Co}^{2+}$  ions form a dimer along  $z$  direction, and these dimers are then organized into a triangular lattice. It can be equivalently viewed as a bilayer triangular lattice, and the interlayer separation is quite short compared to the lattice constant. The magnetic susceptibility and the magnetization measurements clearly indicate the easy-axis spin anisotropy, and the magnetic entropy is consistent with the effective spin-1/2 degree of freedom for each  $\text{Co}^{2+}$  ion. The presence of the 1/3 magnetization plateau is compatible with the predominant Ising interaction or Ising-like moments. Given the previous success of the triangular lattice XXZ model on the spin supersolid compound  $\text{Na}_2\text{BaCo}(\text{PO}_4)_2$  [16–18] and the 120-degree ordered compound  $\text{Ba}_3\text{CoSb}_2\text{O}_9$  [19], we consider an extended XXZ model with the easy-axis anisotropy on this bilayer triangular lattice. In the absence of the magnetic field, the intra-dimer Ising interaction favors the anticollinear spin configuration. Within this manifold, we show that the remaining interactions effectively realize a quantum Ising model on the triangular lattice and then gives rise to the quantum order by disorder effect and the Berezinskii-Kosterlitz-Thouless (BKT) physics at finite temperatures. Although the original XXZ model has a  $U(1)$  symmetry, the emergent BKT physics has no connection with the  $U(1)$  spin symmetry of the spin model. For the magnetic excitations and the magnetization plateau states, the states out of the intra-dimer anticollinear spin states are naturally involved. After incorporating these “excited” collinear states in Fig. 1(b), we end up with the Kugel-Khomskii-like model and thus deal with the Kugel-Khomskii (KK) physics.

To explore the interplay between geometrical frustration and anisotropic interaction, we first write down the extended XXZ model with the spin-1/2 moments on the dimer triangular lattice,

$$H = H_0 + H_u + H_d + H_{ud} + H_Z, \quad (1)$$

where the five different terms are given as

$$H_0 = \sum_i [J_0^z S_{ui}^z S_{di}^z + J_0^\perp (S_{ui}^x S_{di}^x + S_{ui}^y S_{di}^y)], \quad (2)$$

$$H_u = \sum_{\langle ij \rangle} [J_1^z S_{ui}^z S_{uj}^z + J_1^\perp (S_{ui}^x S_{uj}^x + S_{ui}^y S_{uj}^y)], \quad (3)$$

$$H_d = \sum_{\langle ij \rangle} [J_1^z S_{di}^z S_{dj}^z + J_1^\perp (S_{di}^x S_{dj}^x + S_{di}^y S_{dj}^y)], \quad (4)$$

$$H_{ud} = \sum_{\langle ij \rangle} [J_2^z S_{ui}^z S_{dj}^z + J_2^\perp (S_{ui}^x S_{dj}^x + S_{ui}^y S_{dj}^y)] \\ + [J_2^z S_{di}^z S_{uj}^z + J_2^\perp (S_{di}^x S_{uj}^x + S_{di}^y S_{uj}^y)], \quad (5)$$

$$H_Z = \sum_i -B(S_{ui}^z + S_{di}^z). \quad (6)$$

Here  $H_0$  is the intra-dimer interaction,  $H_u$  is the inter-dimer interaction within the up layer,  $H_d$  is the inter-dimer interaction within the down layer,  $H_{ud}$  is the inter-dimer interaction between the up and down layers, and  $H_Z$  is the Zeeman coupling for the field along the  $z$  direction. The spin operator  $S_{ui}^\mu$  ( $S_{di}^\mu$ ) refers to the spin component  $\mu$  at the site  $i$  from the up (down) layer of the dimer triangular lattice. The spin interactions are labeled in Fig. 1(a).

From the lattice geometry, the intra-dimer interaction should be dominant. From the easy-axis anisotropy, the intra-dimer Ising interaction  $J_0^z$  is stronger than the  $xy$  exchange  $J_0^\perp$ . Thus, throughout this work, we will treat the intra-dimer Ising interaction as the dominant interaction. For the inter-dimer interaction, we still consider the easy-axis anisotropy. Moreover, we expect  $J_1^z \gg J_2^z$  from the different exchange paths.

We consider the zero-field case. The ground states of the intra-dimer Ising interaction are doubly degenerate for each dimer, and we introduce an effective pseudospin-1/2 states to label them as

$$|\tau_i^z = +\frac{1}{2}\rangle = |S_{ui}^z = +\frac{1}{2}, S_{di}^z = -\frac{1}{2}\rangle, \quad (7)$$

$$|\tau_i^z = -\frac{1}{2}\rangle = |S_{ui}^z = -\frac{1}{2}, S_{di}^z = +\frac{1}{2}\rangle. \quad (8)$$

We define a projection operator to this reduced local

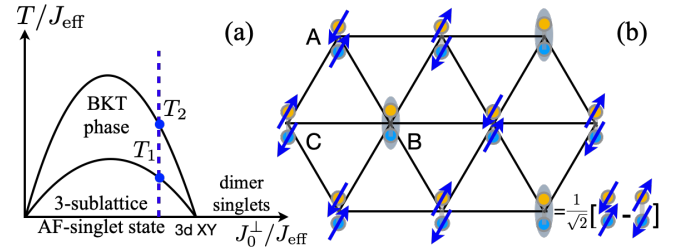


FIG. 2. (a) The phase diagram of quantum Ising model in Eq. (9) (adapted from Ref. 20), where  $J_{\text{eff}} = 2(J_1^z - J_2^z)$ . (b) The 3-sublattice AF-singlet state in the limit of weak transverse field for the dimer triangular lattice.

Hilbert space,  $P = \prod_i \sum_\alpha |\tau_i^z = \alpha\rangle \langle \tau_i^z = \alpha|$ . The effective model in this reduced Hilbert space is  $H_{\text{eff}} = PHP$ . Different spin operators in this reduced Hilbert space is expressed in Tab. I. The effective model is given as a quantum Ising model with

$$H_{\text{eff}} = \sum_i J_0^\perp \tau_i^x + \sum_{\langle ij \rangle} 2(J_1^z - J_2^z) \tau_i^z \tau_j^z - \frac{NJ_0^z}{4}, \quad (9)$$

where  $N$  is the total number of dimers. This is a good approximation as long as  $J_0^z$  is large enough. Remarkably, the inter-dimer transverse exchanges all disappear in this projection as they do not connect the singlet manifolds of neighboring dimers. Unlike  $\text{CoNb}_2\text{O}_6$  [7–9] and  $\text{BaCo}_2\text{V}_2\text{O}_8$  [10–12] whose transverse field is applied externally, the transverse field here is of the intrinsic origin [21]. From  $H_{\text{eff}}$ , one can obtain many properties of the system. The phase diagram of this model is well-known from Ref. 20 and is adapted to our problem in Fig. 2(a), where we set  $J_{\text{eff}} = 2(J_1^z - J_2^z)$ . There are two phases at zero temperature. With the large transverse field, the ground state is polarized in the negative  $\tau^x$  direction, which is equivalent to the local singlet for each dimer. When the effective exchange becomes large, a 3-sublattice order is favored instead, leading to the Bragg peaks at the  $\mathbf{K}$  points of the Brillouin zone. This 3-sublattice order is better visualized in terms of the original spin configuration instead of the pseudospin  $\tau_i$ . We depict this 3-sublattice spin configuration in the limit of weak transverse field in Fig. 2(b). Since  $\tau^x$  is always polarized by the transverse field, each dimer is generically a mixture of the antiferromagnetic Ising configuration and the valence bond spin singlet. This state is then refereed as 3-sublattice AF-singlet state, and was not previously known. The property in this 3-sublattice state can be captured by a Weiss mean-field theory (MFT) with

$$H_{\text{eff}} \rightarrow H_{\text{MF}} = \sum_i J_0^\perp \tau_i^x + \sum_{\langle ij \rangle} J_{\text{eff}} \tau_i^z \langle \tau_j^z \rangle, \quad (10)$$

where  $\langle \tau_j^z \rangle$  is the mean-field order parameter. The details are discussed in the Supplementary materials [22]. The excitations are plotted in Fig. 3, and there exists a mini-gap in the spectrum. This is known as the pseudo-Goldstone mode that results from the quantum order by disorder effect. The effective model does not have the continuous symmetry and the magnetic order does not break the  $U(1)$  symmetry of the original spin model in Eq. (1), so the excitation spectrum is fully gapped. The mini-gap indicates a weak stability of the ground state against the magnetic field, and thus suggests a tiny magnetization plateau in the weak field limit.

The quantum correction or renormalization of the order parameter is not considered in this MFT and thus the bandwidth of the excitations is enhanced compared to the reality. The overall dispersion does not significantly

depend on the order parameter. The critical value of  $J_0^\perp/J_{\text{eff}}$  in the mean-field theory is 1.5 while the numerical result from quantum Monte Carlo is  $\sim 0.82$  [23, 24]. It is important to mention that the excitations are expressed in the variable of  $\tau_i$ . The  $\tau^z$ - $\tau^z$  correlation should create the magnon excitations as well as two-magnon continuum in the 3-sublattice AF-singlet state, and creates the magnon-like dispersive excitation in the Ising disordered state. The local probe such as NMR and  $\mu\text{SR}$  should also be useful to detect the dynamics in this reduced Hilbert space. The  $\tau^x$  component is the bond operator in terms of the original spin variables and is even under time reversal. A useful probe is likely to be the X-ray pair distribution function measurement.

At finite temperatures above the 3-sublattice AF-singlet phase, the order melts via the two-step process before entering the high-temperature paramagnet (see Fig. 2(a)) [20, 25]. The two finite-temperature phase transitions are of the BKT type, and the precise locations of the transitions,  $T_1$  and  $T_2$  (especially the higher temperature one), might be a bit difficult to detect, and show up as broad peaks in specific heat. Below  $T_1$ , the magnetic order emerges as a rigid order with a clear gap. Between  $T_1$  and  $T_2$ , the system is in a BKT phase with an emergent  $U(1)$  symmetry and the spin correlations are of the power law form. It is an algebraically ordered regime but has no true long-range order with [26]

$$\langle \tau_i^z \tau_j^z \rangle \sim \frac{\cos[\mathbf{Q} \cdot (\mathbf{r}_i - \mathbf{r}_j)]}{|\mathbf{r}_i - \mathbf{r}_j|^{\eta(T)}}, \quad (11)$$

where the wavevector  $\mathbf{Q}$  corresponds to the  $\mathbf{K}$  point, and  $\eta \in (1/9, 1/4)$  is temperature dependent. It was even predicted that, the uniform susceptibility in  $\tau^z$  is singular in the power-law in the zero-field limit if a uniform field is applied to the pseudospin  $\tau^z$  components [27]. This corresponds to a weak  $\Gamma$  point peak in the  $\tau^z$ - $\tau^z$  correlation, and it is not true ferromagnetic order in  $\tau^z$ . If the system is close to the quantum phase transition between the 3-sublattice AF-singlet state and the dimer singlets, the system would be controlled by the critical mode at the finite temperatures, and have a  $T^2$  specific heat.

To obtain the full excitations, we ought to return to the original spin model in Eq. (1). Without losing connection to the effective model in Eq. (9), we incorporate the local excited states in Fig. 1(b) as

$$|\tau_i^z = +\frac{1}{2}, \mu_i^z = +\frac{1}{2}\rangle = |S_{ui}^z = +\frac{1}{2}, S_{di}^z = +\frac{1}{2}\rangle, \quad (12)$$

$$|\tau_i^z = -\frac{1}{2}, \mu_i^z = +\frac{1}{2}\rangle = |S_{ui}^z = -\frac{1}{2}, S_{di}^z = -\frac{1}{2}\rangle, \quad (13)$$

and the ground states in Eq. (7) and Eq. (8) are then treated as  $|\mu_i^z = -1/2\rangle$  with the same  $\tau^z$ 's. In this representation of the local Hilbert space, the spin variables are re-expressed in terms of the pseudospins  $\tau^\mu$  and  $\mu^\nu$  and are listed in Tab. I. The original model in Eq. (1) now becomes

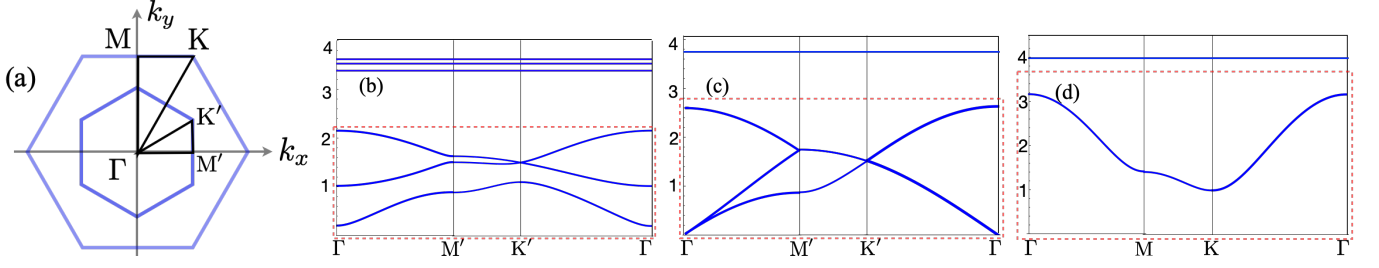


FIG. 3. The full elementary excitations in different zero-temperature phases for the minimal model  $H_{\min}$ . (a) The lattice Brillouin zone and the magnetic Brillouin zone with the high symmetry momentum lines. (b) The elementary excitations in the three sublattice ordered state, where we choose  $J_{\text{eff}} = 1$ ,  $J_0^\perp = 1.1$ ,  $J_0^z = 6$ . (c) The elementary excitations at the criticality, where we choose  $J_{\text{eff}} = 1$ ,  $J_0^\perp = 1.5$ ,  $J_0^z = 6$ . (d) The elementary excitations for the dimer singlet, where we choose  $J_{\text{eff}} = 1$ ,  $J_0^\perp = 2$ ,  $J_0^z = 6$ . The spectra in the (red) dashed box are the elementary excitations for the effective model  $H_{\text{eff}}$  (within the  $\mu^z = -1/2$  manifold), and the rest are excitations out of the  $\mu^z = -1/2$  manifold. The flat excitation would become weakly dispersive once the inter-dimer transverse coupling is included, and the bandwidth of the  $a$ -bosons (i.e. excitations within the  $\mu^z = -1/2$  manifold) should be suppressed by the renormalized order parameter.

$$\begin{aligned}
 H = & \sum_i \left[ \frac{1}{2} J_0^z \mu_i^z + J_0^\perp \tau_i^x \left( \frac{1}{2} - \mu_i^z \right) \right] + \sum_{\langle ij \rangle} \left[ 4J_1^z \tau_i^z \tau_j^z \left( \frac{1}{4} + \mu_i^z \mu_j^z \right) + 4J_1^\perp \left[ \left( \frac{1}{4} + \tau_i^x \tau_j^x \right) \mu_i^x \mu_j^x + \tau_i^y \tau_j^y \mu_i^x \mu_j^x + \tau_i^z \tau_j^z \mu_i^y \mu_j^y \right] \right] \\
 & + \sum_{\langle ij \rangle} \left[ 2J_2^z \tau_i^z \tau_j^z (\mu_i^z + \mu_j^z) + 4J_2^\perp \left[ \frac{1}{2} (\tau_i^x + \tau_j^x) \mu_i^x \mu_j^x + \tau_i^y \tau_j^y \mu_i^x \mu_j^y + \tau_i^z \tau_j^z \mu_i^y \mu_j^x \right] \right] - \sum_i B \tau_i^z (1 + 2\mu_i^z). \quad (14)
 \end{aligned}$$

It is in the form of the Kugel-Khomskii model except that the local degrees of freedom are from the dimer instead of the spin and orbitals [28]. Thus, the system belongs to the so-called “multiflavor Mott insulator” [29]. Based on this model, one can proceed and calculate the full excitations of the 3-sublattice AF-singlet state as well as the dimer singlet state. The presence of  $J_1^\perp, J_2^\perp$  couplings may generate more phases if they become comparable to the Ising exchanges. To avoid further complication, we set  $J_1^\perp = J_2^\perp = 0$  as they might be weaker compared to their corresponding Ising couplings. The simplified model is the minimal model for our calculation below and is given as

$$H_{\min} = \sum_i \left[ \frac{1}{2} J_0^z \mu_i^z + J_0^\perp \tau_i^x \left( \frac{1}{2} - \mu_i^z \right) \right] + \sum_{\langle ij \rangle} \left[ J_1^z \tau_i^z \tau_j^z (1 + 4\mu_i^z \mu_j^z) + 2J_2^z \tau_i^z \tau_j^z (\mu_i^z + \mu_j^z) \right] - \sum_i B \tau_i^z (1 + 2\mu_i^z). \quad (15)$$

We would like to explain why we introduce the effective model first and then deal with the full model or the minimal model in terms of different spin variables. By directly examining the original full model in Eq. (1) and/or the minimal model in Eq. (15), one cannot extract much useful results. After the proper organization of the active Hilbert space and the definition/introduction of new effective variables, one could then make the connection with the effective quantum Ising model on the triangular lattice [24, 30, 31]. These procedures are the most insightful parts, and luckily the system is organized in such a remarkable way to naturally yield the effective model where the hidden physics can be revealed. The results of the 3-sublattice AF-singlet state, BKT physics, 3D XY quantum criticality, *et al* are all straightforward consequences from these procedures and observations.

With the useful results from  $H_{\text{eff}}$ , we analyze  $H_{\min}$  at zero field. Since  $J_0^z$  is a very high energy scale and the  $\mu_i^z = 1/2$  states are high in energy, the ground state phase diagram is not altered. A bit more careful rea-

soning could solve  $H_{\min}$  by separating it into mutually-coupled  $\mu$ -channel model and  $\tau$ -channel model, and then obtain the ground states in this Kugel-Khomskii type of mean-field approaches [22]. The  $\mu$ -channel model gives the ground states with  $\mu_i^z = -1/2$  on each site, and the  $\tau$ -channel model is identical to  $H_{\text{eff}}$  and thus has the same ground states. This treatment does not involve completely throwing away or projecting out the  $\mu_i^z = 1/2$  states and thus does not require a very strong  $J_0^z$ .

To obtain the excitations, we turn to the flavor-wave theory and make the detailed comparison with the linear spin-wave theory [22]. The linear spin-wave theory only captures the separate spin flips of  $\tau$  and  $\mu$ . The linear flavor-wave theory has one extra mode per sublattice beyond the linear spin-wave theory by including the spin flipping process of for both  $\tau$  and  $\mu$ . For the 3-sublattice AF-singlet state, 9 flavor bosons are introduced. Keeping the quadratic terms in the bosons for the minimal model, we obtain the linear flavor-wave model as

$$H_{\text{fw}} = H_{\text{fw}\tau} + H_{\text{fw}\mu} + H_{\text{fw}\tau\mu}, \quad (16)$$

$$\begin{aligned}
H_{\text{fw}\tau} &= \sum_{\mathbf{k}, \mu\nu} [\mathcal{A}_{\mathbf{k}, \mu\nu} a_{\mathbf{k}\mu}^\dagger a_{\mathbf{k}\nu} + (\mathcal{B}_{\mathbf{k}, \mu\nu} a_{\mathbf{k}\mu}^\dagger a_{-\mathbf{k}\nu}^\dagger + h.c.)], \\
H_{\text{fw}\mu} &= \sum_{\mathbf{k}} \left( \frac{J_0^z - sJ_0^\perp}{2} \sum_{\mu \neq \text{B}} b_{\mathbf{k}\mu}^\dagger b_{\mathbf{k}\mu} + \frac{J_0^z + J_0^\perp}{2} b_{\mathbf{k}\text{B}}^\dagger b_{\mathbf{k}\text{B}} \right), \\
H_{\text{fw}\tau\mu} &= \sum_{\mathbf{k}} \left( \frac{J_0^z - sJ_0^\perp}{2} + \frac{3}{4} c^2 J_{\text{eff}} \right) \sum_{\mu \neq \text{B}} c_{\mathbf{k}\mu}^\dagger c_{\mathbf{k}\mu} \\
&\quad + \sum_{\mathbf{k}} \frac{J_0^z + J_0^\perp}{2} c_{\mathbf{k}\text{B}}^\dagger c_{\mathbf{k}\text{B}},
\end{aligned}$$

where  $\mu, \nu$  refer to the sublattices,  $\mathbf{k}$  is summed over the magnetic Brillouin zone,  $s = \sin \theta$  and  $c = \cos \theta$  associate with the orientation of the magnetic order, and we have the relation [22]  $\mathcal{A}_{\mathbf{k}, \mu\nu} = \mathcal{A}_{\mathbf{k}, \nu\mu}^*$ ,  $\mathcal{B}_{\mathbf{k}, \mu\nu} = \mathcal{B}_{\mathbf{k}, \nu\mu}^*$ .

In  $H_{\text{fw}}$ , the spin dynamics within and out of the  $\mu^z = -1/2$  manifold is decoupled.  $H_{\text{fw}\tau}$  describes the  $\tau$  dynamics within the  $\mu^z = -1/2$  manifold that is identical to the one for the effective model  $H_{\text{eff}}$ .  $H_{\text{fw}\mu}$  and  $H_{\text{fw}\mu\tau}$  describe the spin fluctuations out of the  $\mu^z = -1/2$  manifold. The full excitations of the 3-sublattice AF-singlet state are plotted in Fig. 3(b), as well as the ones at the critical point in Fig. 3(c). In Fig. 3(b), the presence of the  $\langle \tau^z \rangle$  order split the excitations out of the  $\mu^z = -1/2$  manifold [22]. With the similar and simpler approaches, we further established the full excitations for the dimer singlet in Fig. 3(d), and the excitations within and out of the  $\mu^z = -1/2$  manifold become separately degenerate.

*Discussion.*—We have obtained the key properties of the spin model for a dimer triangular lattice antiferromagnet by properly organizing the local spin Hilbert space and defining new sets of pseudospin variables. The hidden physics is then revealed with these variables. The full model can be thought as the quantum Ising model of the pseudospin- $\tau$  decorated with the pseudospin- $\mu$ , and is solved with the mean-field approach and supplied with the existing understanding. This kind of decorated spin models with two distinct spins is potentially related to the decorated domain/string realizations of symmetry-protected topological orders [32, 33]. In this work, we have mainly dealt with the zero-field case, the characteristic quantum excitations of each quantum phase are established. Although the transformation into the new sets of spin operators makes a great simplification of the problem, the appearance of the original spin operators becomes rather complex and behaves differently for different spin variables. This may cause some complication in the interpretation of the spectroscopic measurement. For both the 3-sublattice AF-singlet state and the dimer singlet, the excitations within and out of the  $\mu^z = -1/2$  manifold are well separated from the separation of  $a, b, c$  bosons in Eq. (16). From the relations of the physical spins and the flavor-wave bosons, the excitations of the  $a, b, c$  bosons can be detected with inelastic neutron scattering as the well-defined flavor-wave modes. For the 3-sublattice AF-singlet state, a subtle feature should occur.

As the system orders in  $\tau^z$ , this longitudinal component correlation naturally involves the 2-boson continuum of the  $a$ -bosons [22].

Due to the strong Ising anisotropy, the system is expected to support the magnetization plateau. This is realized when the Zeeman energy gain overcomes the dimer singlet formation and the subdominant exchange energy remains optimized or nearly optimized. Unlike the quantum Ising model on the triangular lattice where the magnetic field simply lifts the degeneracy of the up-up-down and down-down-up spin configurations on the triangular plaquettes and does not alter the Ising exchange, here due to the extra  $\mu$ -spin degrees of freedom and the bilayer triangular geometry, the polarization of the spin dimer from the singlet to the triplet actually “quenches” the neighboring exchange bonds, generating the emergent lattices. The resulting plateau states are briefly discussed [22]. Finally, since our minimal model does not have the fermion sign problem for the quantum Monte Carlo simulation, we expect more quantitative information to be established in later numerical simulation.

*Acknowledgments.*—We would like to thank Tong Chen for very recent communication. This work is supported by the National Science Foundation of China with Grant No. 92065203 and by the Ministry of Science and Technology of China with Grants No. 2021YFA1400300, and by the Fundamental Research Funds for the Central Universities, Peking University.

- 
- [1] C. Lacroix, P. Mendels, and F. Mila, *Introduction to Frustrated Magnetism: Materials, Experiments, Theory* (2011).
  - [2] W. Witczak-Krempa, G. Chen, Y. B. Kim, and L. Balents, Correlated Quantum Phenomena in the Strong Spin-Orbit Regime, *Annual Review of Condensed Matter Physics* **5**, 57–82 (2014).
  - [3] H. Takagi, T. Takayama, G. Jackeli, G. Khaliullin, and S. E. Nagler, Concept and realization of Kitaev quantum spin liquids, *Nature Reviews Physics* **1**, 264–280 (2019).
  - [4] J. G. Rau and M. J. Gingras, Frustrated Quantum Rare-Earth Pyrochlores, *Annual Review of Condensed Matter Physics* **10**, 357–386 (2019).
  - [5] H. Liu and G. Khaliullin, Pseudospin exchange interactions in  $d^7$  cobalt compounds: Possible realization of the Kitaev model, *Phys. Rev. B* **97**, 014407 (2018).
  - [6] R. Sano, Y. Kato, and Y. Motome, Kitaev-Heisenberg Hamiltonian for high-spin  $d^7$  Mott insulators, *Phys. Rev. B* **97**, 014408 (2018).
  - [7] R. Coldea, D. A. Tennant, E. M. Wheeler, E. Wawrzynska, D. Prabhakaran, M. Telling, K. Habicht, P. Smeibidl, and K. Kiefer, Quantum Criticality in an Ising Chain: Experimental Evidence for Emergent  $E_8$  Symmetry, *Science* **327**, 177–180 (2010).
  - [8] A. W. Kinross, M. Fu, T. J. Munsie, H. A. Dabkowska, G. M. Luke, S. Sachdev, and T. Imai, Evolution of Quantum Fluctuations Near the Quantum Critical Point of

- the Transverse Field Ising Chain System  $\text{CoNb}_2\text{O}_6$ , *Phys. Rev. X* **4**, 031008 (2014).
- [9] C. M. Morris, N. Desai, J. Viirrok, D. H  vonen, U. Nagel, T. R    m, J. W. Krizan, R. J. Cava, T. M. McQueen, S. M. Koohpayeh, R. K. Kaul, and N. P. Armitage, Duality and domain wall dynamics in a twisted Kitaev chain, *Nature Physics* **17**, 832–836 (2021).
- [10] Z. Wang, T. Lorenz, D. I. Gorbunov, P. T. Cong, Y. Kohama, S. Niesen, O. Breunig, J. Engelmayer, A. Herman, J. Wu, K. Kindo, J. Wosnitza, S. Zherlitsyn, and A. Loidl, Quantum Criticality of an Ising-like Spin-1/2 Antiferromagnetic Chain in a Transverse Magnetic Field, *Phys. Rev. Lett.* **120**, 207205 (2018).
- [11] S. Suga, Tomonaga–Luttinger Liquid in Quasi-One-Dimensional Antiferromagnet  $\text{BaCo}_2\text{V}_2\text{O}_8$  in Magnetic Fields, *Journal of the Physical Society of Japan* **77**, 074717 (2008).
- [12] Z. Wang, J. Wu, W. Yang, A. K. Bera, D. Kamenskyi, A. T. M. N. Islam, S. Xu, J. M. Law, B. Lake, C. Wu, and A. Loidl, Experimental observation of Bethe strings, *Nature* **554**, 219–223 (2018).
- [13] Y. Cui, H. Zou, N. Xi, Z. He, Y. X. Yang, L. Shu, G. H. Zhang, Z. Hu, T. Chen, R. Yu, J. Wu, and W. Yu, Quantum Criticality of the Ising-like Screw Chain Antiferromagnet  $\text{SrCo}_2\text{V}_2\text{O}_8$  in a Transverse Magnetic Field, *Phys. Rev. Lett.* **123**, 067203 (2019).
- [14] H. Zou, Y. Cui, X. Wang, Z. Zhang, J. Yang, G. Xu, A. Okutani, M. Hagiwara, M. Matsuda, G. Wang, G. Mussardo, K. H  ds  gi, M. Kormos, Z. He, S. Kimura, R. Yu, W. Yu, J. Ma, and J. Wu,  $E_8$  Spectra of Quasi-One-Dimensional Antiferromagnet  $\text{BaCo}_2\text{V}_2\text{O}_8$  under Transverse Field, *Phys. Rev. Lett.* **127**, 077201 (2021).
- [15] R. Zhong, S. Guo, L. T. Nguyen, and R. J. Cava, Frustrated spin-1/2 dimer compound  $\text{K}_2\text{Co}_2(\text{SeO}_3)_3$  with easy-axis anisotropy, *Phys. Rev. B* **102**, 224430 (2020).
- [16] J. Sheng, L. Wang, A. Candini, W. Jiang, L. Huang, B. Xi, J. Zhao, H. Ge, N. Zhao, Y. Fu, J. Ren, J. Yang, P. Miao, X. Tong, D. Yu, S. Wang, Q. Liu, M. Kofu, R. Mole, G. Biasiol, D. Yu, I. A. Zaliznyak, J.-W. Mei, and L. Wu, Two-dimensional quantum universality in the spin-1/2 triangular-lattice quantum antiferromagnet  $\text{Na}_2\text{BaCo}(\text{PO}_4)_2$ , *Proceedings of the National Academy of Sciences* **119**, e2211193119 (2022).
- [17] J. Xiang, C. Zhang, Y. Gao, W. Schmidt, K. Schmalzl, C.-W. Lu, B. Li, N. Xi, X.-Y. Liu, H. Jin, G. Li, J. Shen, Z. Chen, Y. Qi, Y. Wan, W. Jin, W. Li, P. Sun, and G. Su, Giant magnetocaloric effect in spin supersolid candidate  $\text{Na}_2\text{BaCo}(\text{PO}_4)_2$ , *Nature* **625**, 270 (2024).
- [18] H. Jia, B. Ma, Z. Wang, and G. Chen, Quantum spin supersolid as a precursory dirac spin liquid in a triangular lattice antiferromagnet (2023), [arXiv:2304.11716 \[cond-mat.str-el\]](https://arxiv.org/abs/2304.11716).
- [19] J. Ma, Y. Kamiya, T. Hong, H. B. Cao, G. Ehlers, W. Tian, C. D. Batista, Z. L. Dun, H. D. Zhou, and M. Matsuda, Static and Dynamical Properties of the Spin-1/2 Equilateral Triangular-Lattice Antiferromagnet  $\text{Ba}_3\text{CoSb}_2\text{O}_9$ , *Phys. Rev. Lett.* **116**, 087201 (2016).
- [20] R. Moessner and S. L. Sondhi, Ising models of quantum frustration, *Phys. Rev. B* **63**, 224401 (2001).
- [21] G. Chen, Intrinsic transverse field in frustrated quantum Ising magnets: Physical origin and quantum effects, *Phys. Rev. Res.* **1**, 033141 (2019).
- [22] See the Supplementary materials for more information.
- [23] S. V. Isakov and R. Moessner, Interplay of quantum and thermal fluctuations in a frustrated magnet, *Phys. Rev. B* **68**, 104409 (2003).
- [24] C. Liu, C.-J. Huang, and G. Chen, Intrinsic quantum Ising model on a triangular lattice magnet  $\text{TmMgGaO}_4$ , *Phys. Rev. Res.* **2**, 043013 (2020).
- [25] J. V. Jos  , L. P. Kadanoff, S. Kirkpatrick, and D. R. Nelson, Renormalization, vortices, and symmetry-breaking perturbations in the two-dimensional planar model, *Phys. Rev. B* **16**, 1217 (1977).
- [26] K. Damle, Melting of Three-Sublattice Order in Easy-Axis Antiferromagnets on Triangular and Kagome Lattices, *Phys. Rev. Lett.* **115**, 127204 (2015).
- [27] S. Biswas and K. Damle, Singular ferromagnetic susceptibility of the transverse-field Ising antiferromagnet on the triangular lattice, *Phys. Rev. B* **97**, 085114 (2018).
- [28] F. Mila, Low-Energy Sector of the  $S = 1/2$  Kagome Antiferromagnet, *Phys. Rev. Lett.* **81**, 2356 (1998).
- [29] G. Chen and C. Wu, Multiflavor Mott insulators in quantum materials and ultracold atoms, *npj Quantum Materials* **9**, 1 (2021).
- [30] Y. Shen, C. Liu, Y. Qin, S. Shen, Y.-D. Li, R. Bewley, A. Schneidewind, G. Chen, and J. Zhao, Intertwined dipolar and multipolar order in the triangular-lattice magnet  $\text{TmMgGaO}_4$ , *Nature Communications* **10**, 10.1038/s41467-019-12410-3 (2019).
- [31] J. c. v. Chaloupka, Emergent transverse-field Ising model in  $d^4$  spin-orbit Mott insulators, *Phys. Rev. B* **109**, L020403 (2024).
- [32] L. Savary, Quantum loop states in spin-orbital models on the honeycomb lattice, *Nature Communications* **12** (2021).
- [33] X. Chen, Y.-M. Lu, and A. Vishwanath, Symmetry-protected topological phases from decorated domain walls, *Nature Communications* **5**, 10.1038/ncomms4507 (2014).

# Supplementary materials for “Emergent Berezinskii-Kosterlitz-Thouless and Kugel-Khomskii physics in the triangular lattice bilayer colbaltate”

Gang V. Chen\*

International Center for Quantum Materials, School of Physics, Peking University, Beijing 100871, China and Collaborative Innovation Center of Quantum Matter, 100871, Beijing, China

## I. MEAN-FIELD THEORY FOR THE EFFECTIVE MODEL

This section is devoted to explaining the mean-field treatment for the effective model  $H_{\text{eff}}$  in the main text. For the three-sublattice AF-singlet state, we introduce the mean-field order parameters in Tab. II. In fact, this assignment of the order parameters captures both the three-sublattice AF-singlet state and the dimer singlet (or the Ising disordered state). When  $\theta = -\pi/2$ , the system is in the dimer singlet.

	$\langle \tau_i^z \rangle$	$\langle \tau_i^x \rangle$
$i \in \text{A sublattice}$	$\frac{1}{2} \cos \theta$	$\frac{1}{2} \sin \theta$
$i \in \text{B sublattice}$	0	$-\frac{1}{2}$
$i \in \text{C sublattice}$	$-\frac{1}{2} \cos \theta$	$\frac{1}{2} \sin \theta$

TABLE I. The mean-field order parameters for each sublattices in the 3-sublattice AF-singlet phase. Here  $\theta < 0$ .

In the Weiss mean-field treatment,  $H_{\text{eff}}$  is reduced to

$$\begin{aligned}
 H_{\text{MF}} &= \sum_i J_0^\perp \tau_i^x + \sum_{\langle ij \rangle} J_{\text{eff}} \tau_i^z \langle \tau_j^z \rangle \\
 &= \sum_{i \in \text{A}} \left[ J_0^\perp \tau_i^x - \frac{3}{2} J_{\text{eff}} \cos \theta \tau_i^z \right] + \sum_{i \in \text{B}} J_0^\perp \tau_i^x \\
 &+ \sum_{i \in \text{C}} \left[ J_0^\perp \tau_i^x + \frac{3}{2} J_{\text{eff}} \cos \theta \tau_i^z \right], \quad (2)
 \end{aligned}$$

where all the three sublattices are effectively decoupled. The self-consistent mean-field equations for the A and C sublattices are the same. The self-consistent mean-field equation for the B sublattice is automatically solved as  $\tau_i^x = -1/2$ . The self-consistent mean-field equation for  $i \in \text{A}$  is then given as

$$\langle \tau_i^z \rangle = \frac{\frac{3}{4} J_{\text{eff}} \cos \theta}{\left[ \left( \frac{3}{2} J_{\text{eff}} \cos \theta \right)^2 + (J_0^\perp)^2 \right]^{1/2}}, \quad (3)$$

which yields the critical value of  $J_0^\perp / J_{\text{eff}}$  as 1.5. The numerical value was found to be  $\sim 0.82$  [1, 2]. To capture the essential and qualitative physics and be consistent

throughout, we stick to the mean-field calculation and explain the quantitative aspect afterwards based on the physical understanding.

## II. LINEAR SPIN-WAVE THEORY FOR THE EFFECTIVE MODEL

In this section, we perform the linear spin-wave theory to solve for the excitations of the effective model  $H_{\text{eff}}$  in the 3-sublattice AF-singlet state and the dimer singlet.

### A. Three-sublattice AF-singlet state

For both A and C sublattices, the pseudospin vectors point away from  $x$  and  $z$  directions, and we need to choose the quantization axis to be aligned with the ordered moment in the Holstein-Primarkoff spin wave representation. In the linear spin-wave formulation, the pseudospin operators are represented as

$$\begin{cases} \tau_i^x = +\frac{1}{2} \cos \theta (a_{iA}^\dagger + a_{iA}) + \sin \theta (\frac{1}{2} - a_{iA}^\dagger a_{iA}), \\ \tau_i^z = -\frac{1}{2} \sin \theta (a_{iA}^\dagger + a_{iA}) + \cos \theta (\frac{1}{2} - a_{iA}^\dagger a_{iA}), \end{cases} \quad (4)$$

for  $i \in \text{A sublattice}$ ,

$$\begin{cases} \tau_i^x = -\frac{1}{2} + a_{iB}^\dagger a_{iB}, \\ \tau_i^z = -\frac{1}{2} (a_{iB}^\dagger + a_{iB}), \end{cases} \quad (5)$$

for  $i \in \text{B sublattice}$ , and

$$\begin{cases} \tau_i^x = -\frac{1}{2} \cos \theta (a_{iC}^\dagger + a_{iC}) + \sin \theta (\frac{1}{2} - a_{iC}^\dagger a_{iC}), \\ \tau_i^z = -\frac{1}{2} \sin \theta (a_{iC}^\dagger + a_{iC}) - \cos \theta (\frac{1}{2} - a_{iC}^\dagger a_{iC}), \end{cases} \quad (6)$$

for  $i \in \text{C sublattice}$ . According to the specification in Fig. 1, there are three intra-magnetic cell couplings and twelve inter-magnetic cell couplings. Keeping the quadratic terms in the bosons and properly grouping these terms, we obtain the linear spin wave theory,

$$\begin{aligned}
 H_{\text{eff}} \rightarrow & \sum_{\mathbf{k}} \sum_{\mu\nu} a_{\mathbf{k}\mu}^\dagger a_{\mathbf{k}\nu} \mathcal{A}_{\mu\nu}(\mathbf{k}) + a_{\mathbf{k}\mu}^\dagger a_{-\mathbf{k}\nu}^\dagger \mathcal{B}_{\mu\nu}(\mathbf{k}) \\
 & + a_{\mathbf{k}\mu}^\dagger a_{-\mathbf{k}\nu}^\dagger \mathcal{B}_{\mu\nu}^*(\mathbf{k}) \quad (7)
 \end{aligned}$$

where  $\mu, \nu = \text{A, B, C}$ , and the boson hoppings and pairings are given as

\* Away from University of Hong Kong

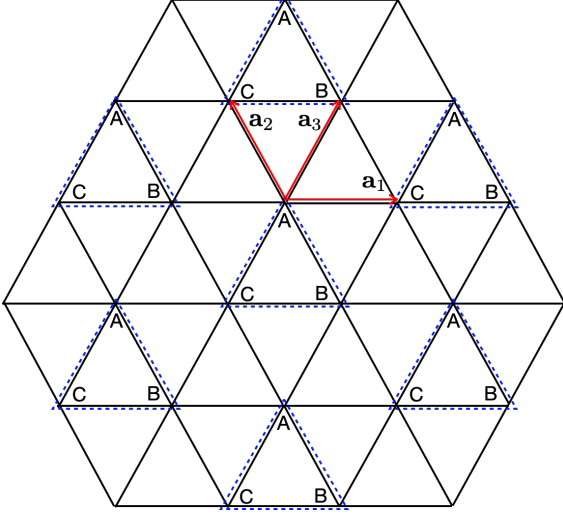


FIG. 1. The specification of magnetic sublattices and magnetic unit cells. The dashed triangle specifies the magnetic unit cell such that the intra- and inter- magnetic unit cell couplings become clear. The vectors  $\mathbf{a}_1, \mathbf{a}_2, \mathbf{a}_3$  are three nearest-neighbor vectors of the triangular lattice.

$$\mathcal{A}_{11}(\mathbf{k}) = -J_0^\perp \sin \theta + \frac{3}{2} J_{\text{eff}} \cos^2 \theta, \quad (8)$$

$$\mathcal{A}_{22}(\mathbf{k}) = J_0^\perp, \quad (9)$$

$$\mathcal{A}_{33}(\mathbf{k}) = -J_0^\perp \sin \theta + \frac{3}{2} J_{\text{eff}} \cos^2 \theta \quad (10)$$

$$\mathcal{A}_{12}(\mathbf{k}) = \frac{J_{\text{eff}}}{4} \sin \theta (e^{-i\mathbf{k} \cdot \mathbf{a}_1} + e^{-i\mathbf{k} \cdot \mathbf{a}_2} + e^{i\mathbf{k} \cdot \mathbf{a}_3}), \quad (11)$$

$$\mathcal{A}_{13}(\mathbf{k}) = \frac{J_{\text{eff}}}{4} \sin^2 \theta (e^{i\mathbf{k} \cdot \mathbf{a}_1} + e^{i\mathbf{k} \cdot \mathbf{a}_2} + e^{-i\mathbf{k} \cdot \mathbf{a}_3}), \quad (12)$$

$$\mathcal{A}_{23}(\mathbf{k}) = \frac{J_{\text{eff}}}{4} \sin \theta (e^{-i\mathbf{k} \cdot \mathbf{a}_1} + e^{-i\mathbf{k} \cdot \mathbf{a}_2} + e^{i\mathbf{k} \cdot \mathbf{a}_3}), \quad (13)$$

and

$$\mathcal{B}_{12}(\mathbf{k}) = \frac{J_{\text{eff}}}{4} \sin \theta (e^{-i\mathbf{k} \cdot \mathbf{a}_1} + e^{-i\mathbf{k} \cdot \mathbf{a}_2} + e^{i\mathbf{k} \cdot \mathbf{a}_3}), \quad (14)$$

$$\mathcal{B}_{13}(\mathbf{k}) = \frac{J_{\text{eff}}}{4} \sin^2 \theta (e^{i\mathbf{k} \cdot \mathbf{a}_1} + e^{i\mathbf{k} \cdot \mathbf{a}_2} + e^{-i\mathbf{k} \cdot \mathbf{a}_3}), \quad (15)$$

$$\mathcal{B}_{23}(\mathbf{k}) = \frac{J_{\text{eff}}}{4} \sin \theta (e^{-i\mathbf{k} \cdot \mathbf{a}_1} + e^{-i\mathbf{k} \cdot \mathbf{a}_2} + e^{i\mathbf{k} \cdot \mathbf{a}_3}). \quad (16)$$

### B. Dimer singlet state

For the dimer singlet, there is only one sublattice, and the spin-wave representation is much simpler and is given as

$$\begin{cases} \tau_i^x = -\frac{1}{2} + a_i^\dagger a_i, \\ \tau_i^z = -\frac{1}{2} (a_i^\dagger + a_i), \end{cases} \quad (17)$$

and the linear spin-wave Hamiltonian is then obtained as

$$H_{\text{eff}} \rightarrow \frac{J_{\text{eff}}}{4} \sum_{\mathbf{k}} \sum_{\mu} \cos(\mathbf{k} \cdot \mathbf{a}_{\mu}) (a_{\mathbf{k}} a_{-\mathbf{k}} + a_{\mathbf{k}}^\dagger a_{-\mathbf{k}}^\dagger + 2a_{\mathbf{k}}^\dagger a_{\mathbf{k}}) + J_0^\perp \sum_{\mathbf{k}} a_{\mathbf{k}}^\dagger a_{\mathbf{k}}, \quad (18)$$

where the momentum summation is over the Brillouin zone of the triangular lattice. The excitation spectrum is ready to be solved and is given as

$$\epsilon_{\mathbf{k}} = 2 \left[ \left( \sum_{\mu} \frac{1}{4} J_{\text{eff}} \cos(\mathbf{k} \cdot \mathbf{a}_{\mu}) + \frac{1}{2} J_0^\perp \right)^2 - \left( \sum_{\mu} \frac{1}{4} J_{\text{eff}} \cos(\mathbf{k} \cdot \mathbf{a}_{\mu}) \right)^2 \right]^{1/2}. \quad (19)$$

The dispersion arises from the effective exchange  $J_{\text{eff}}$ , and becomes flat when  $J_{\text{eff}} \rightarrow 0$ .

### III. MEAN-FIELD THEORY FOR THE MINIMAL MODEL

We extend the mean-field treatment for the effective model  $H_{\text{eff}}$  to the minimal model  $H_{\text{min}}$ . This mean-field treatment requires extra steps. One can actually adopt some experiences from the Kugel-Khomskii spin-orbital exchange model where one can decouple the full model into the mutually-dependent spin and orbital mean-field models. Here, we decouple the minimal model  $H_{\text{min}}$  with coupled pseudospin  $\tau_i$  and  $\mu_j$  into the mutually-dependent mean-field models, and the models are given as

$$H_{\mu\text{MF}} = \sum_i \frac{1}{2} J_0^z \mu_i^z + J_0^\perp \langle \tau_i^x \rangle \left( \frac{1}{2} - \mu_i^z \right) + \sum_{\langle ij \rangle} \langle \tau_i^z \tau_j^z \rangle \times [J_1^z (1 + 4\mu_i^z \mu_j^z) + 2J_2^z (\mu_i^z + \mu_j^z)], \quad (20)$$

$$H_{\tau\text{MF}} = \sum_i J_0^\perp \tau_i^x \left[ \frac{1}{2} - \langle \mu_i^z \rangle \right] + \sum_{\langle ij \rangle} \tau_i^z \tau_j^z \times [J_1^z (1 + 4\langle \mu_i^z \mu_j^z \rangle) + 2J_2^z (\langle \mu_i^z \rangle + \langle \mu_j^z \rangle)]. \quad (21)$$

Since  $J_0^z$  is the dominant energy scale,  $H_{\mu\text{MF}}$  can be viewed as the Ising model with non-uniform Ising couplings in a strong “magnetic field”. The Ising coupling depends on the bond correlation  $\langle \tau_i^z \tau_j^z \rangle$ .  $H_{\tau\text{MF}}$  should be viewed as a transverse field Ising model with the bond-dependent exchange couplings and site-dependent local transverse field.

Here we explain that  $\mu_i^z$  should be polarized to  $-1/2$ . First of all, a strong “magnetic field” of  $J_0^z$  should already be sufficient to polarize the pseudospin  $\mu_i^z$  as  $\mu_i^z = -1/2$ . Nevertheless, one can further soften the condition. From  $H_{\tau\text{MF}}$ , the effective transverse field on  $\tau^x$  is always positive. This is due to the fact that

$$\frac{1}{2} - \langle \mu_i^z \rangle > 0. \quad (22)$$

The extreme case with  $\mu_i^z = 1/2$  cannot happen as it is disfavored by a large  $J_0^z$ . Thus we have  $\langle \tau_i^x \rangle < 0$  throughout. In order to optimize the second term alone in  $H_{\mu\text{MF}}$ , we should require  $\mu_i^z = -1/2$ . The analysis of the third term in  $H_{\mu\text{MF}}$  requires the knowledge of  $\langle \tau_i^z \tau_j^z \rangle$  that can be considered from  $H_{\tau\text{MF}}$ . Although a strong  $J_0^z$  would be sufficient to force  $\langle \mu_i^z \rangle = -1/2$ , since we are now softening this condition, a not-so-strong  $J_0^z$  would simply favor a uniform  $\langle \mu_i^z \rangle < 0$  with the support of the second term in  $H_{\mu\text{MF}}$ . This indicates that

$$\begin{cases} J_1^z[1 + 4\langle \mu_i^z \mu_j^z \rangle] > J_1^z, \\ -2J_2^z \leq 2J_2^z[\langle \mu_i^z \rangle + \langle \mu_j^z \rangle] < 0. \end{cases} \quad (23)$$

From the exchange path and distances, it is expected that  $J_1^z \gg J_2^z$ . Thus,  $H_{\tau\text{MF}}$  is the quantum Ising model with the antiferromagnetic exchange, and this generally favors  $\langle \tau_i^z \tau_j^z \rangle < 0$ . Thus, in the third term of  $H_{\mu\text{MF}}$ , the exchange coupling is ferromagnetic, and the overall coefficient of the  $J_2$  term is ferromagnetic. Since  $J_2$  is small, it cannot flip the sign of the total effective magnetic field for  $\mu_i^z$ . Thus, one can safely conclude that

$$\mu_i^z = -\frac{1}{2}. \quad (24)$$

for all sites even if the dominant energy scale  $J_0^z$  is reduced.

With Eq. (24), the mean-field model  $H_{\tau\text{MF}}$  immediately becomes  $H_{\text{eff}}$ . Alternatively, one could simply set  $\mu_i^z = -\frac{1}{2}$  in the original minimal model  $H_{\text{min}}$ . The outcome is the same. But to obtain this outcome, one has to go through the above explanation.

#### IV. LINEAR SPIN-WAVE THEORY FOR THE MINIMAL MODEL

Since the pseudospin  $\mu_i^z = -1/2$  throughout the parameter regime of our interest, the Holstein-Primarkoff boson representation is the same in both 3-sublattice AF-singlet state and the Ising disordered state for the minimal model. We replace the pseudospin operator  $\mu_i$  as

$$\mu_i^z = -\frac{1}{2} + b_i^\dagger b_i, \quad (25)$$

and there is no other transverse component involved in  $H_{\text{min}}$ . For the full model with finite  $J_1^\perp$  and  $J_2^\perp$ , the transverse components are needed.

##### A. Three sublattice order in the minimal model

For the 3-sublattice AF-singlet state, the  $\tau$ -spins are represented in the same way as prescribed in Sec. II A. As the transverse component of  $\mu$  spins is not involved in  $H_{\text{min}}$ , no dispersion is created. The resulting linear

spin-wave model for the 3-sublattice AF-singlet is given as

$$H_{\text{sw}} = H_{\text{sw}\tau} + H_{\text{sw}\mu}, \quad (26)$$

where  $H_{\text{sw}\tau}$  is identical to the one in Sec. II A, and  $H_{\text{sw}\mu}$  is given as

$$\begin{aligned} H_{\text{sw}\mu} = \sum_{\mathbf{k}} & \left[ \frac{1}{2}(J_0^z - J_0^\perp \sin \theta)(b_{\mathbf{kA}}^\dagger b_{\mathbf{kA}} + b_{\mathbf{kC}}^\dagger b_{\mathbf{kC}}) \right. \\ & \left. + \frac{1}{2}(J_0^z + J_0^\perp)b_{\mathbf{kB}}^\dagger b_{\mathbf{kB}} \right], \end{aligned} \quad (27)$$

where the summation of the momentum is over the magnetic Brillouin zone. This creates three flat bands of  $\mu$ -sector excitations on top of the  $\tau$ -sector excitations. Among these three flat bands, two are degenerate.

##### B. Dimer singlet state in the minimal model

For the dimer singlet state, the  $\tau$  component is represented in the same way as the expression in Eq. (17), and the minimal model is reduced to the spin wave model as

$$\begin{aligned} H_{\text{min}} \rightarrow & \frac{J_{\text{eff}}}{4} \sum_{\mathbf{k}} \sum_{\mu} \cos(\mathbf{k} \cdot \mathbf{a}_\mu)(a_{\mathbf{k}} a_{-\mathbf{k}} + a_{\mathbf{k}}^\dagger a_{-\mathbf{k}}^\dagger + 2a_{\mathbf{k}}^\dagger a_{\mathbf{k}}) \\ & + \sum_{\mathbf{k}} J_0^\perp a_{\mathbf{k}}^\dagger a_{\mathbf{k}} + \sum_{\mathbf{k}} \frac{1}{2}(J_0^z + J_0^\perp)b_{\mathbf{k}}^\dagger b_{\mathbf{k}}, \end{aligned} \quad (28)$$

where a flat excitation of the  $\mu$  sector with the energy  $\frac{1}{2}(J_0^z + J_0^\perp)$  is introduced on top of the excitation of the effective model  $H_{\text{eff}}$ .

#### V. LINEAR FLAVOR-WAVE THEORY FOR THE MINIMAL MODEL

In this section, we implement the linear flavor-wave theory for the minimal model. The linear spin-wave theory for the minimal model captures the linear spin-flipping process of both  $\tau$  and  $\mu$  pseudospins separately, but does not capture the process of flipping  $\tau$  and  $\mu$  at the same time in the linear order. If one examines the spin operator such as  $S_{ui}^x$  that is equal to  $2\tau_i^x \mu_i^x$  in Tab. 1 of the main text, this spin operator would flip  $\tau^z$  and  $\mu^z$  simultaneously. To capture this part of excitation, a bit more complete treatment is to rely on the linear flavor-wave theory.

In fact, as we have viewed this system as one example of “multiflavor Mott insulators”, the key property of “multiflavor Mott insulators” is that the system is more delocalized on the local Hilbert space and allows the quantum tunneling from one local state to all other local states at the linear order of the Hamiltonian [3]. For such systems when they are ordered, the linear flavor-wave theory is more appropriate than the linear spin-wave theory by capturing more relevant modes of excitations at

the linear level. In the following, we first implement the linear flavor-wave theory for the dimer singlet and then solve the excitations for the 3-sublattice AF-singlet state.

### A. Linear flavor-wave theory for the dimer singlet

We describe the flavor-wave treatment for the dimer singlet here. A more complicated version can be straightforwardly obtained for the 3-sublattice AF-singlet state. The dimer singlet is a direct product state where every site can be described by the same wavefunction,

$$|\text{dimer singlet}\rangle \approx \prod_i |\tau_i^x = -\frac{1}{2}, \mu_i^z = -\frac{1}{2}\rangle_i. \quad (29)$$

Thus, we choose our basis for the flavor-wave bosons as

$$|0\rangle_i \equiv a_{i0}^\dagger |\emptyset\rangle \equiv |\tau_i^x = -\frac{1}{2}, \mu_i^z = -\frac{1}{2}\rangle, \quad (30)$$

$$|1\rangle_i \equiv a_{i1}^\dagger |\emptyset\rangle \equiv |\tau_i^x = +\frac{1}{2}, \mu_i^z = -\frac{1}{2}\rangle, \quad (31)$$

$$|2\rangle_i \equiv a_{i2}^\dagger |\emptyset\rangle \equiv |\tau_i^x = -\frac{1}{2}, \mu_i^z = +\frac{1}{2}\rangle, \quad (32)$$

$$|3\rangle_i \equiv a_{i3}^\dagger |\emptyset\rangle \equiv |\tau_i^x = +\frac{1}{2}, \mu_i^z = +\frac{1}{2}\rangle, \quad (33)$$

where  $|\emptyset\rangle$  is the vacuum state. A Hilbert space constraint on every site is imposed with

$$a_{i0}^\dagger a_{i0} + a_{i1}^\dagger a_{i1} + a_{i2}^\dagger a_{i2} + a_{i3}^\dagger a_{i3} = 1. \quad (34)$$

The physical spin operators can be expressed as the bilinears of the flavor-wave bosons. For example,  $S_{ui}^x$  is given as

$$S_{ui}^x \equiv \sum_{m,n} i \langle m | S_{ui}^x | n \rangle_i a_{im}^\dagger a_{in}, \quad (35)$$

where  $m, n = 0, 1, 2, 3$ .

For the dimer singlet, the  $a_0$  boson is condensed with

$$\begin{aligned} \langle a_0^\dagger \rangle = \langle a_{i0} \rangle &= \sqrt{1 - a_{i1}^\dagger a_{i1} - a_{i2}^\dagger a_{i2} - a_{i3}^\dagger a_{i3}} \\ &\approx 1. \end{aligned} \quad (36)$$

The relevant spin operators in the minimal model can then be obtained as

$$\tau_i^x \left( \frac{1}{2} - \mu_i^z \right) \approx -\frac{1}{2} + a_{i1}^\dagger a_{i1} + \frac{1}{2} (a_{i2}^\dagger a_{i2} + a_{i3}^\dagger a_{i3}) \quad (37)$$

$$\tau_i^z \mu_i^z \approx \frac{1}{4} (a_{i1} + a_{i1}^\dagger), \quad (38)$$

$$\tau_i^z \approx -\frac{1}{2} (a_{i1} + a_{i1}^\dagger), \quad (39)$$

$$\tau_i^x \approx -\frac{1}{2} + a_{i1}^\dagger a_{i1} + a_{i3}^\dagger a_{i3}, \quad (40)$$

$$\mu_i^z \approx -\frac{1}{2} + a_{i2}^\dagger a_{i2} + a_{i3}^\dagger a_{i3}. \quad (41)$$

One can make a direct comparison with the linear spin-wave theory in Sec. II and Sec. IV, and identify that

$$a_i = a_{i1}, \quad b_i = a_{i2}. \quad (42)$$

Thus, to simplify the notation, we let  $a_{i3} = c_i$  and continue to use the notations of  $a_i$  and  $b_i$ .

In this formulation of the linear flavor-wave theory, the minimal model is reduced to

$$\begin{aligned} H_{\min} \rightarrow & \frac{J_{\text{eff}}}{4} \sum_{\mathbf{k}} \sum_{\mu} \cos(\mathbf{k} \cdot \mathbf{a}_{\mu}) (a_{\mathbf{k}} a_{-\mathbf{k}} + a_{\mathbf{k}}^\dagger a_{-\mathbf{k}}^\dagger + 2a_{\mathbf{k}}^\dagger a_{\mathbf{k}}) \\ & + \sum_{\mathbf{k}} J_0^\perp a_{\mathbf{k}}^\dagger a_{\mathbf{k}} + \sum_{\mathbf{k}} \frac{1}{2} (J_0^z + J_0^\perp) (b_{\mathbf{k}}^\dagger b_{\mathbf{k}} + c_{\mathbf{k}}^\dagger c_{\mathbf{k}}). \end{aligned} \quad (43)$$

In comparison with the linear spin-wave theory in Eq. (28), the linear flavor-wave theory model has one extra  $c$ -boson whose energy is identical to the  $b$ -boson.

### B. Linear flavor-wave theory for the three-sublattice AF-singlet state

Here we turn to the linear flavor-wave theory for the 3-sublattice AF-singlet state. Here we describe the formulation for the A sublattice, and the C sublattice lattice is then obtained from the A sublattice by simply setting  $\theta \rightarrow \pi - \theta$ . For the B sublattice, since the local state is a dimer singlet, we simply use the formulation of the previous subsection.

For  $i \in \text{A sublattice}$ , we define the flavor-wave bosons as

$$|0\rangle_i \equiv a_{iA0}^\dagger |\emptyset\rangle \equiv |\tilde{\tau}_i^z = +\frac{1}{2}, \mu_i^z = -\frac{1}{2}\rangle, \quad (44)$$

$$|1\rangle_i \equiv a_{iA1}^\dagger |\emptyset\rangle \equiv |\tilde{\tau}_i^z = -\frac{1}{2}, \mu_i^z = -\frac{1}{2}\rangle, \quad (45)$$

$$|2\rangle_i \equiv a_{iA2}^\dagger |\emptyset\rangle \equiv |\tilde{\tau}_i^z = +\frac{1}{2}, \mu_i^z = +\frac{1}{2}\rangle, \quad (46)$$

$$|3\rangle_i \equiv a_{iA3}^\dagger |\emptyset\rangle \equiv |\tilde{\tau}_i^z = -\frac{1}{2}, \mu_i^z = +\frac{1}{2}\rangle, \quad (47)$$

and supplement with the Hilbert space constraint

$$a_{iA0}^\dagger a_{iA0} + a_{iA1}^\dagger a_{iA1} + a_{iA2}^\dagger a_{iA2} + a_{iA3}^\dagger a_{iA3} = 1, \quad (48)$$

where  $\tilde{\tau}_i^z \equiv \cos \theta \tau_i^z + \sin \theta \tau_i^x$ , and

$$|\tilde{\tau}_i^z = +\frac{1}{2}\rangle = \cos \frac{\theta}{2} |\tau_i^z = \frac{1}{2}\rangle + \sin \frac{\theta}{2} |\tau_i^z = -\frac{1}{2}\rangle, \quad (49)$$

$$|\tilde{\tau}_i^z = -\frac{1}{2}\rangle = -\sin \frac{\theta}{2} |\tau_i^z = \frac{1}{2}\rangle + \cos \frac{\theta}{2} |\tau_i^z = -\frac{1}{2}\rangle \quad (50)$$

For the A sublattice,  $a_{iA0}$  is condensed, and we can approximately have

$$\langle a_{iA0} \rangle = \langle a_{iA0}^\dagger \rangle \approx 1, \quad (51)$$

and the relevant spin operators for the A sublattice are given as

$$\mu_i^z = -\frac{1}{2} + a_{iA2}^\dagger a_{iA2} + a_{iA3}^\dagger a_{iA3}, \quad (52)$$

$$\begin{aligned}
\tau_i^x \left( \frac{1}{2} - \mu_i^z \right) &= \frac{1}{2} \sin \theta + \frac{1}{2} \cos \theta (a_{iA1}^\dagger + a_{iA1}) - \sin \theta a_{iA1}^\dagger a_{iA1} \\
&\quad - \frac{1}{2} \sin \theta (a_{iA2}^\dagger a_{iA2} + a_{iA3}^\dagger a_{iA3}), \\
\tau_i^z &= \frac{1}{2} \cos \theta - \cos \theta (a_{iA1}^\dagger a_{iA1} + a_{iA3}^\dagger a_{iA3}) \\
&\quad - \frac{1}{2} \sin \theta (a_{iA1}^\dagger + a_{iA1}), \\
\tau_i^z \mu_i^z &= -\frac{1}{4} \cos \theta + \frac{1}{2} \cos \theta (a_{iA1}^\dagger a_{iA1} + a_{iA2}^\dagger a_{iA2}) \\
&\quad + \frac{1}{4} \sin \theta (a_{iA1}^\dagger + a_{iA1}).
\end{aligned} \tag{53}$$

## VI. THE SPIN COMPONENTS IN THE FLAVOR-WAVE BOSONS

In this section, we clarify the relations between the physical spins and the flavor-wave bosons in the linear flavor-wave approximation. These relations are particularly useful to understand the experimental signatures in the inelastic neutron scattering measurements. In the actual experiments, the experimental apparatus is directly coupled to the physical spins, instead of the effective pseudospins. This is our motivation to establish these relations.

A comparison with Sec. II and Sec. IV, one can infer that

$$a_{iA} = a_{iA1}, \quad b_{iA} = a_{iA2}. \tag{56}$$

Likewise, for the B and C sublattices, we have

$$a_{iB} = a_{iB1}, \quad b_{iB} = a_{iB2}, \tag{57}$$

$$a_{iC} = a_{iC1}, \quad b_{iC} = a_{iC2}. \tag{58}$$

With the above representation of the spin operators, we reduce the minimal model into the linear flavor-wave model as

$$H_{\text{fw}} = H_{\text{fw}\tau} + H_{\text{fw}\mu} + H_{\text{fw}\tau\mu}. \tag{59}$$

Since we have identified the relation between the flavor-wave boson and the spin-wave boson, we then can identify the relation on the model side and have

$$H_{\text{fw}\tau} = H_{\text{sw}\tau}, \tag{60}$$

$$H_{\text{fw}\mu} = H_{\text{sw}\mu}. \tag{61}$$

$H_{\text{fw}\tau\mu}$  is a new term in the linear flavor-wave theory that arises from the flipping of the both  $\tau$  and  $\mu$  pseudospins, and is given as

$$\begin{aligned}
H_{\text{fw}\tau\mu} &= \sum_{\mathbf{k}} \left( \frac{J_0^z - \sin \theta J_0^\perp}{2} + \frac{3}{4} \cos^2 \theta J_{\text{eff}} \right) \sum_{\mu \neq B} c_{\mathbf{k}\mu}^\dagger c_{\mathbf{k}\mu} \\
&\quad + \sum_{\mathbf{k}} \frac{J_0^z + J_0^\perp}{2} c_{\mathbf{k}B}^\dagger c_{\mathbf{k}B},
\end{aligned} \tag{62}$$

where we have replaced  $a_{iA3}, a_{iB3}, a_{iC3}$  with  $c_{iA}, c_{iB}, c_{iC}$ , respectively. This result has been expressed in the main text. Although a simplified energy in the first line of Eq. (62) can be obtained, we keep the expression that relates to the magnetic order such that the connection to the dimer singlet state can be made. This  $c$ -boson excitation has the same energy as the  $b$ -boson in the dimer singlet state, but differs from the  $b$ -boson in the 3-sublattice AF-singlet state for the A and C sublattices. This is because the presence of the pseudospin  $\tau_i$  order (in the  $z$  component) modulates the excitations from the  $\mu_i^z = -1/2$  manifold to the  $\mu_i^z = 1/2$  manifold. Thus, we observe three flat energy bands in the excitations of the 3-sublattice AF-singlet state in Fig. 3 of the main text.

### A. Dimer singlet

$S_{ui}^z$	$= \tau_i^z$	$\approx -\frac{1}{2}(a_i + a_i^\dagger)$
$S_{ui}^x$	$= 2\tau_i^x \mu_i^x$	$\approx -\frac{1}{2}(b_i + b_i^\dagger)$
$S_{ui}^y$	$= 2\tau_i^y \mu_i^x$	$\approx +\frac{i}{2}(c_i - c_i^\dagger)$
$S_{di}^z$	$= 2\tau_i^z \mu_i^z$	$\approx +\frac{1}{2}(a_i + a_i^\dagger)$
$S_{di}^x$	$= \mu_i^x$	$\approx +\frac{1}{2}(b_i + b_i^\dagger)$
$S_{di}^y$	$= 2\tau_i^z \mu_i^y$	$\approx -\frac{i}{2}(c_i - c_i^\dagger)$

TABLE II. The representation of the physical spin operators in terms of flavor-wave bosons in the dimer singlet. The first column is the physical spin, the second column is in terms of the two pseudospins, and the third column is in the linear flavor-wave boson approximation. Here, we actually keep the flavor-wave bosons up to the quadratic order for the diagonal contribution.

In Tab. II, we list the expression of the physical spin in the linear flavor-wave approximation. Following the expression in Eq. (35), we keep the off-diagonal part to the linear order in the flavor-wave boson and keep the diagonal part to the quadratic order in the flavor-wave boson. One could improve the results by including the high-order off-diagonal part. From Tab. II, one can immediately conclude that all the  $a, b, c$ , flavor bosons should occur as the well-defined flavor-wave modes in the inelastic neutron scattering measurements.

### B. Three-sublattice AF-singlet state

For the 3-sublattice AF-singlet state, we list the results in Tab. III for the A sublattice, and the C sublattice is obtained by setting  $\theta$  to  $\pi - \theta$ . For the B sublattice, we directly adopt the results in Tab. II.

Based on these relations, all the  $a, b, c$ , flavor bosons should occur as the well-defined flavor-wave modes in the inelastic neutron scattering measurements. Moreover, the  $z$ -component spin correlation will involve the  $a$ -boson continuum in the inelastic neutron scattering measurements. The reason is as follows. To diagonalize

$$\begin{aligned}
S_{ui}^z &\approx \frac{1}{2} \cos \theta - \frac{1}{2} \sin \theta (a_{iA} + a_{iA}^\dagger) - \cos \theta (a_{iA}^\dagger a_{iA} + c_{iA}^\dagger c_{iA}) \\
S_{ui}^x &\approx \frac{1}{2} \sin \theta (b_{iA} + b_{iA}^\dagger) + \frac{1}{2} \cos \theta (c_{iA} + c_{iA}^\dagger) \\
S_{ui}^y &\approx -\frac{i}{2} (c_{iA} - c_{iA}^\dagger) \\
S_{di}^z &\approx -\frac{1}{2} \cos \theta + \frac{1}{2} \sin \theta (a_{iA} + a_{iA}^\dagger) + \cos \theta (a_{iA}^\dagger a_{iA} + b_{iA}^\dagger b_{iA}) \\
S_{di}^x &\approx +\frac{1}{2} (b_{iA} + b_{iA}^\dagger) \\
S_{di}^y &\approx +\frac{i}{2} \cos \theta (b_{iA} - b_{iA}^\dagger) - \frac{i}{2} \sin \theta (c_{iA} - c_{iA}^\dagger)
\end{aligned}$$

TABLE III. The representation of the physical spin operators in terms of flavor-wave bosons in the 3-sublattice AF-singlet state for the A sublattice. The first column is the physical spin, and the second column is in the linear flavor-wave boson approximation.

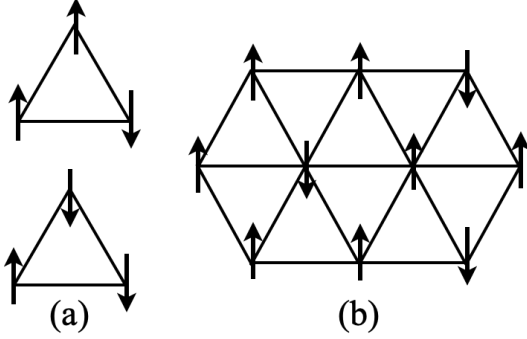


FIG. 2. (a) The degenerate up-up-down and down-down-up spin configurations for the classical Ising model on the triangular plaquette. (b) The 1/3 magnetization plateau state on the triangular lattice.

$H_{\text{fw}\tau}$ , one needs to make a Bogoliubov transformation due to the pairing term. Thus, the action of  $a_i^\dagger a_i$  on the ground state has the zero-point contribution and is non-zero, and the  $z$ -component spin correlation then contains the  $a$ -boson continuum. For the  $b$  or  $c$  bosons, the  $H_{\text{fw}\mu}$  and  $H_{\text{fw}\mu\tau}$  are diagonalized without any transformation. The action of  $b_i^\dagger b_i$  (or  $c_i^\dagger c_i$ ) on the ground state is zero.

## VII. MAGNETIZATION PLATEAU STATES

Here we give a discussion of the magnetization plateau states in the presence of  $z$ -direction magnetic fields. To motivate this discussion, we first sketch the 1/3 magnetization plateau state for the antiferromagnetic Ising model on the triangular lattice under the external magnetic field on the Ising component. The Zeeman coupling over there immediately lifts the degeneracy of the “down-down-up” and “up-up-down” spin configurations for each triangular plaquette (see Fig. 2(a)). Once the “up-up-down” spin configuration is fixed on one triangular plaquette, the spin configuration on the whole triangular lattice is determined (see Fig. 2(b)), and the exchange energy on each triangular plaquette is optimized. Such a “up-up-down”

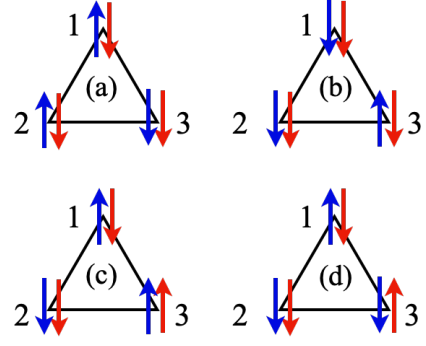


FIG. 3. (a) and (b) are the  $\tau^z$  Ising spin configurations with  $\mu_i^z = -1/2$  throughout on one triangular plaquette. (c) and (d) are the  $\tau^z$  Ising spin configurations by flipping one  $\mu_i^z$  from  $-1/2$  to  $+1/2$ . The blue arrows are for  $\tau^z$  spins, and the red arrows are for  $\mu^z$  spins. The same choice is given for the other figures.

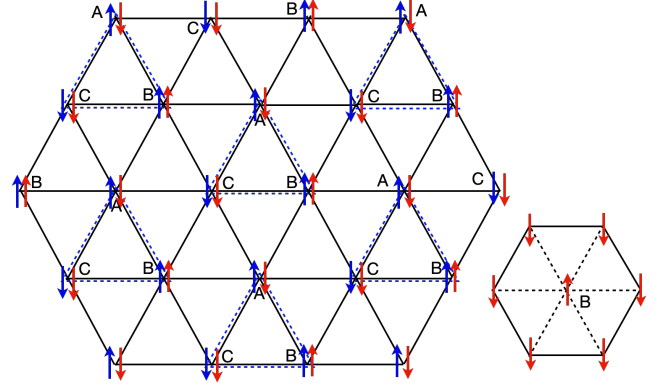


FIG. 4. The spin configuration for the 1/3 magnetization plateau of the minimal model by setting  $J_0^\perp = 0$ . The B sublattice has  $\mu_i^z = 1/2$ . In the inset, the dashed bonds have zero exchange coupling for  $\tau^z$ 's, and the remaining hexagon with even number of bonds is antiferromagnetically coupled for the  $\tau^z$  spins.

state retains the three-sublattice structure and gives rise to the 1/3 magnetization plateau on the triangular lattice. Due to the robustness of this “up-up-down” state, it persists even to the quantum case with the transverse field [2].

For the minimal model  $H_{\text{min}}$ , the local Hilbert space is large, and this is where the complication and difference arise. We consider the classical limit by setting  $J_0^\perp = 0$ , and the regime with  $J_0^z \gg J_1^z \gg J_2^z$ . At the zero magnetic field,  $\mu^z = -1/2$  on every site, and the model is the antiferromagnetic Ising model with  $\tau$  variables. For each triangular plaquette, there exist one unsatisfied bond and two satisfied bonds, and overall there is one net satisfied bonds for the Ising spin interactions of the  $\tau$  spins. This is shown as Figs. 3(a) and (b). When the external magnetic field polarizes one dimer singlet into the dimer triplet by flipping one  $\mu_i^z$  from  $-1/2$  to  $+1/2$ , the exchange coupling on the antiferromagnetically arranged  $\mu^z$  bond is

quenched. In Figs. 3(c) and (d), the exchange interactions on the 13 and 23 bonds are zero, and the remaining 23 bond is optimized. Thus, the net satisfied bond on the triangular plaquette remains to be one. The spin state in Fig. 3(d) does not gain Zeeman energy for the positive- $\hat{z}$  magnetic field compared to the spin state in Fig. 3(c) because the total magnetization on the site 3 is down. Once the Zeeman energy gain of the spin state in Fig. 3(c) overcomes the singlet-triplet energy gap  $J_0^z/2$ , then the spin state is satisfied. To make sure only one  $\mu_i^z$  spin to be flipped for each triangular plaquette for the whole triangular lattice, one arrange the  $\mu^z = 1/2$  sites in a next-nearest neighbor fashion, which is very much like the “up” spin of the  $1/3$  magnetization state in Fig. 2(b).

As we show in Fig. 4, the B sites have  $\mu^z = 1/2, \tau_i^z = 1/2$  to gain the Zeeman energy, and are decoupled from the remaining sites due to the quenched exchange interactions. The remaining sites have  $\mu^z = -1/2$  and form an emergent honeycomb lattice that are unfrustrated (see the inset of Fig. 4). These sites have an antiferromagnetically arranged  $\tau^z$  spin configuration, and there is no extensive or subextensive degeneracy any more. The magnetization of this state is solely contributed from the B sites and is equal to  $1/3$  of the fully polarized state. Due to the robustness of this state, the system should have the  $1/3$  magnetization plateau for this state. As it is depicted in Fig. 4, this state retains the three-sublattice structure. If one further increases the magnetic field, more plateau states will be generated.

- 
- [1] S. V. Isakov and R. Moessner, Interplay of quantum and thermal fluctuations in a frustrated magnet, [Phys. Rev. B \*\*68\*\*, 104409 \(2003\)](#).  
 [2] C. Liu, C.-J. Huang, and G. Chen, Intrinsic quantum Ising

- model on a triangular lattice magnet TmMgGaO<sub>4</sub>, [Phys. Rev. Res. \*\*2\*\*, 043013 \(2020\)](#).  
 [3] G. Chen and C. Wu, Multiflavor Mott insulators in quantum materials and ultracold atoms, [npj Quantum Materials \*\*9\*\*, 1 \(2021\)](#).